Microfluidic Investigation Reveals Distinct Roles for Actin Cytoskeleton and Myosin II Activity in Capillary Leukocyte Trafficking

Sylvain Gabriele, Anne-Marie Benoliel, Pierre Bongrand, and Olivier Théodoly*
Université de la Méditerranée, Institut National de la Santé et de la Recherche Médicale INSERM U600-Centre National de la Recherche Scientifique CNRS UMR6212, Marseille, France

ABSTRACT Circulating leukocyte sequestration in pulmonary capillaries is arguably the initiating event of lung injury in acute respiratory distress syndrome. We present a microfluidic investigation of the roles of actin organization and myosin II activity during the different stages of leukocyte trafficking through narrow capillaries (entry, transit and shape relaxation) using specific drugs (latrunculin A, jasplakinolide, and blebbistatin). The deformation rate during entry reveals that cell stiffness depends strongly on F-actin organization and hardly on myosin II activity, supporting a microfilament role in leukocyte sequestration. In the transit stage, cell friction is influenced by stiffness, demonstrating that the actin network is not completely broken after a forced entry into a capillary. Conversely, membrane unfolding was independent of leukocyte stiffness. The surface area of sequestered leukocytes increased by up to 160% in the absence of myosin II activity, showing the major role of molecular motors in microvilli wrinkling and zipping. Finally, cell shape relaxation was largely independent of both actin organization and myosin II activity, whereas a deformed state was required for normal trafficking through capillary segments.

INTRODUCTION

The mechanical plugging of lung microvessels by leukocytes has been implicated in the pathophysiology of several diseases, such as acute lung injury (ALI). The estimated 190,000 cases of ALI in the United States generate high costs, and acute respiratory distress syndrome (ARDS), the most hypoxemic ALI presentation, results in a mortality rate ranging from 34% to 58% (1). ARDS is a challenging entity for clinical investigation because it lacks an accepted diagnostic test and relies on a panel of clinical findings for diagnosis. Leukocyte sequestration has been reported after sepsis, trauma, hemorrhagic shock, or ischemia (2), and sequestration in lung microvasculature is considered as the initiating event in the development of ARDS (3).

It is difficult to study the mechanisms of leukocyte sequestration (adhesion and/or low deformability) in humans. Recent evidence demonstrates that the initial stages of neutrophil sequestration in rats are not due to CD11-CD18 mediated adhesion, supporting a major involvement of leukocyte mechanical properties in sequestration (4). Also, leukocyte mechanical behavior was investigated with the use of many techniques aimed at quantifying leukocyte deformability and rheology under various conditions, including cell poker (5), polycarbonate filter (6), parallel plates (7), atomic force microscopy (8), optical tweezers (9), microrheometry, and micropipette aspiration (10). Although power law rheology behavior and associated models are gaining ground (11,12), there is no universal understanding of the precise role of the three major filamentous constituents of the cytoskeleton—microtubules (10), intermediate filaments (13), and actin filaments (14)—in leukocyte mechanical properties. Actin filaments appear to be a primary structural determinant of neutrophil mechanical properties (14). Furthermore, Nishino and co-workers (15) demonstrated that neutrophils from patients with septic shock and ARDS were significantly more rigid than controls, and observed a change in actin network polymerization. Evidence for the formation of an actin-rich rim in the submembrane region of deformed (16) and ARDS patient (15) leukocytes raises questions regarding the precise role of actin microfilament organization in the mechanical changes of circulating leukocytes (17). On the other hand, Lämmermann and co-workers (18) recently demonstrated that myosin II-dependent contraction of migrating leukocytes was required for passage through narrow gaps, suggesting an important contribution of molecular motors in the behavior of leukocytes sequestered in narrow capillaries. These results underline the importance of investigating the precise roles of actin and actomyosin activity in capillary leukocyte trafficking.

Significant insights into the rheological properties of model leukocytes in microcapillaries, such as HL60 or THP-1 cells, have been obtained by micropipette aspiration, but only in the first stage of leukocyte entry into constriction. Additional information on subsequent stages (capillary transit and shape recovery) under physiologically relevant hydrodynamical conditions is needed. The versatility of microfluidics allows physiologically relevant testing on the whole passage process (16,19) and may be more relevant to clinical problems.

Here, we present an efficient microfluidic approach to measure new relevant parameters of leukocyte transit in narrow capillaries, such as entry time (ET), cell velocity in

Submitted November 26, 2008, and accepted for publication February 17, 2009.

*Correspondence: olivier.theodoly@inserm.fr

Sylvain Gabriele's present address is Université de Mons-Hainaut, Mons, Belgique.

Editor: Denis Wirtz.

0006-3495/09/05/4308/11 $2.00

doi: 10.1016/j.bpj.2009.02.037

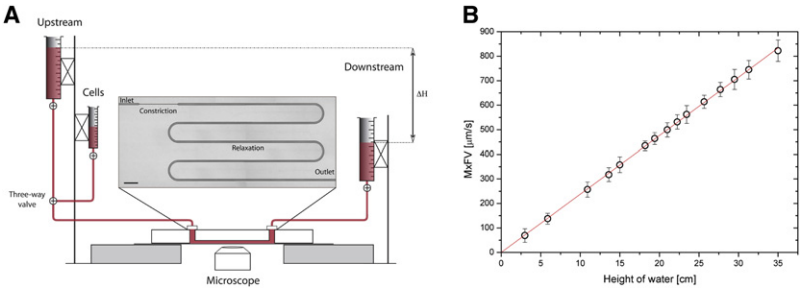

FIGURE 1 Microfluidic setup. (*A*) Pressure drops were imposed by varying the height of water, ΔH, between the upstream and downstream macroreservoirs. Cells were introduced into the device by a syringe connected to the upstream reservoir with a three-way valve. The inset shows a picture of the 4-μm-wide constriction channel (length: 2250 μm) and 20-μm-wide inlet/oulet channels. Scale bar corresponds to 850 μm. (*B*) Maximum fluid velocity measured by fluorescent particles tracking, MxFV, versus ΔH. Values are mean $\pm$ SE; $n = 4$.

constriction, cell morphology during capillary transit through a constriction, shape recovery kinetics after passage, and the effect of a first deformation on the passage through successive segments. We intend to define the specific role of actin cytoskeleton and actomyosin activity in the passage of circulating leukocytes through narrow capillaries. To that end, we specifically enhanced or inhibited actin cytoskeleton and actomyosin activity. We used actin-specific agents with well-described molecular effects: latrunculin A (LatA), a potent microfilament inhibitor (20); jasplakinolide (Jpk), which stabilizes actin filaments (21); and blebbistatin (Blb), which specifically inhibits myosin II activity in leukocytes (22). We confirm the important influence of actin filament organization on the deformation rate in the entry stage. Our results also provide what we believe are new insights into the roles of actin cytoskeleton and myosin II activity during the transit stage. Cell velocity in the constriction is lower because the actin network is more organized, and cell membrane unfolding is controlled by myosin II activity. In the relaxation stage after release from the constriction, we found that actin organization and molecular motor activity did not influence the shape recovery process, and that a deformed shape helps normal trafficking through successive capillary segments.

MATERIALS AND METHODS

Cell preparation and drug treatments

We used the monocytic THP-1 line (23) maintained as previously described (24) in Roswell Park Memorial Institute-1640 medium (Invitrogen, Cergy Pontoise, France) supplemented with 20 mM HEPES buffer, 10% fetal calf serum (FCS), 2 mM L-glutamine, 50 U/mL penicillin, and 50 μg/mL streptomycin. Stock cell cultures were passaged twice weekly and maintained at 37°C in a humidified atmosphere containing 5% CO_2. Cell diameter was determined by cytometry at a mean of 12.5 μm with a standard deviation (SD) of 0.75 μm. Jpk (J7473, 1.4 mM; Molecular Probes, Eugene, OR), LatA (L12370, 2.37 mM; Molecular Probes, Eugene, OR), and Blb (75 mM; Fischer Bioblock Scientific, Illkirch, France) stock solutions were prepared in dimethyl sulfoxide (DMSO) and stored at −20°C. Cells (1×10^6/mL) were incubated at 37°C with Jpk, LatA, and Blb at concentrations of 3, 3, and 50 μg/mL, respectively, on a rocking platform for 20 min for Blb (25) and 30 min for Jpk and LatA (26). Control experiments showed that DMSO up to 0.5% does not affect THP-1 mechanical properties, and additional experiments performed 30 min after the exposition period demonstrated that the effects of these drugs were sustained for the entire experimental period.

Microfluidic setup

Microfluidic channels were drawn using Clewin software (WieWeb Software, Hengelo, The Netherlands) and a chromium mask (Toppan Photomask, Corbeil Essonnes, France) was then generated. Using standard soft lithography procedures (27), a master of channels was fabricated on a silicon wafer by photolithography with photosensitive resins (SU-8 2015; Microchem, Newton, MA) and microfluidic channels were molded with polydimethylsiloxane (PDMS, Sylgard 184 Silicone Elastomer Kit; Dow Corning, Midland, MI). Ports to plug the inlet and outlet reservoirs were punched in the PDMS replica with a gauge needle. The device was finalized by sealing the PDMS piece on 170-μm-thick glass coverslips via O_2-plasma activation of both surfaces, and all channels were incubated with a 1% pluronic F108 solution (BASF, Mount Olive, NJ) for 2 h to deter cell adhesion. Inlet and outlet reservoirs were connected to the microfluidic device with Teflon tubings and the reservoirs were attached to a linear translation stage mounted on a linear slide. Pressure drops across the microchannel were controlled by varying the height between inlet and outlet macroreservoirs (Fig. 1 *A*). Observations were made with an inverted microscope (Olympus IX71) equipped with an oil objective of magnification ×100 (UplanFLN 1.30; Olympus, Tokyo, Japan).

Our device is composed of an inlet channel, a 4-μm-wide constriction channel, and a relaxation channel (Fig. 1 *A*). All channels have the same height H of 16 μm, and all experiments were performed with cells of selected diameter $D_i = 12 \pm 0.5$ μm. Geometrically, a spherical cell of diameter D_i squeezed at constant volume in a slit of width W is deformed into a puck of height W and diameter D_{pu}:

$$D_{pu} = \sqrt{\frac{2D_i^3}{3W}}. \quad (1)$$

In our experiments, $D_i = 12$ μm and $W = 4$ μm (Eq. 1) give $D_{pu} = 17$ μm. Given that $H = 16$ μm, undeformed cells travel freely in the inlet and relaxation channels, and squeezed cells in the constriction at minimum deformation fill the full cross-section area of the constriction. The latter condition ensures that the pressure drop across the constriction applies fully to cells with minimum fluid leakage around them.

RESULTS

Microfluidic experiments

A typical experiment consists of video-recording the different stages of a single cell crossing the 4-μm-wide constriction, i.e., entry, transit, and shape recovery after release (see Movie S1 in the Supporting Material). The constraint applied to the cells corresponds to physiological flow conditions maintained by applying constant hydrostatic pressure. A calibration was performed by tracking fluorescent micron-size particles in the constriction to measure the maximum fluid velocity, MxFV, against the applied pressure

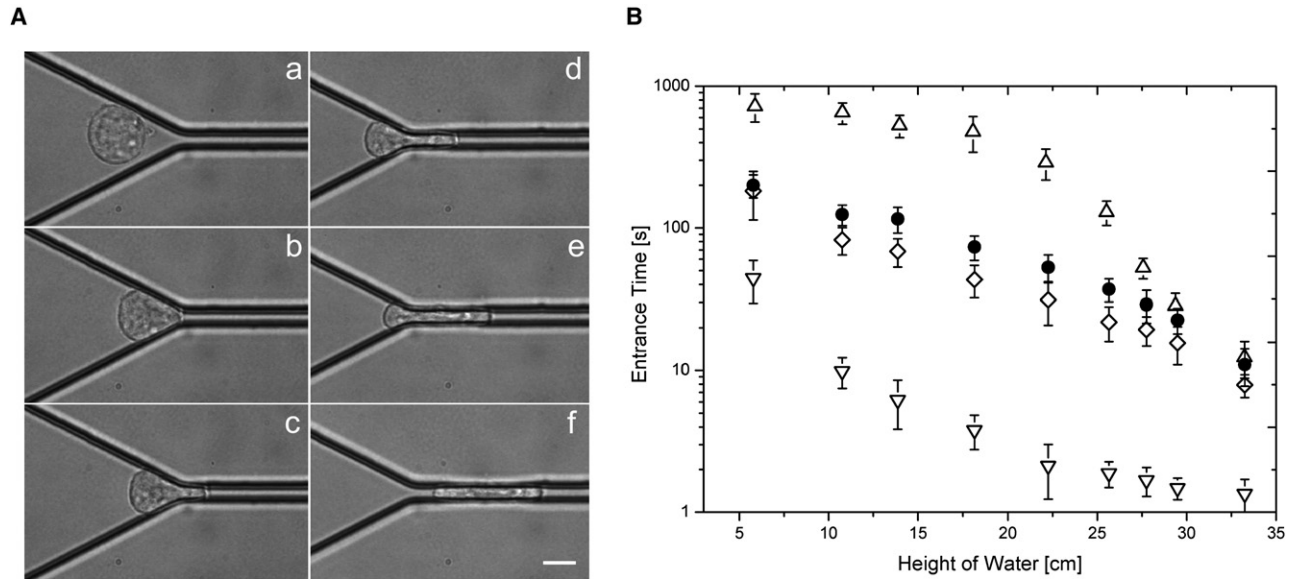

FIGURE 2 Entry stage. (*A*) Image sequence of a Blb-treated THP-1 cell during entry into the 4-μm-wide constriction ($\Delta H = 10.8$ cm H_2O); (*a*) approach, (*b*) contact, (*c*), (*d* and *e*) development of a projection in the constriction, and (*f*) completed entry. The scale bar represents 12 μm. (*B*) ETs versus height of water, ΔH, for normal (●), Blb-treated (◇), Jpk-treated (△), and LatA-treated (▽) THP-1 cells. Error bars represent SE (THP-1: $n = 7$; LatA: $n = 4$; Jpk: $n = 4$; Blb: $n = 6$).

ΔH between the inlet and outlet reservoirs (Fig. 1 *B*). The local pressure drop across the constriction is 10-fold smaller than ΔH.

Cell ETs are dependent on actin cytoskeleton organization

Fig. 2 *A* shows a typical sequence of the deformation displayed by a THP-1 cell entering the narrow capillary. The cell projection length versus the time in the constriction entry stage follows a sigmoidal curve (Fig. S1). Cell deformability can also be assessed by measuring the time required for cells to enter the constriction. We defined the ET as the time interval between the leading edge of the cell crossing the entry into the microchannel and its trailing edge clearing the entry. Serial single-cell ET measurements as a function of applied driving pressures (Fig. 2 *B*) were taken 30 min after exposure to Jpk and LatA. Generally, the ET decreases with driving pressure and the dependency of ET on cell treatments is enhanced at low driving pressures. Jpk-treated cells exhibited very long ETs of >700 s at low ΔH (6 cm H_2O), ~3-fold higher than controls. Conversely, the average ET at low ΔH of LatA-treated cells was ~2 times lower than the ETs of controls. Further, the ETs observed for Blb-treated cells exhibited only minor differences from controls. Thus, the ETs of cells in a narrow capillary are affected mainly by the passive actin cytoskeleton organization and marginally by molecular motor activity.

Cell velocity in constriction depends on the actin cytoskeleton

The cell velocity was constant all along the 2250-μm-long constriction. The mean cell velocity, MnCV, was determined using the time interval between the trailing edge of the cell clearing the entry and its leading edge clearing the constriction. The mean fluid velocity, MnFV, was calculated using the measured maximum velocity MxFV and the theoretical flow profile in our microchannels (28). Fig. 3 *A* shows the evolution of MnCV/MnFV ratios as a function of the applied driving pressure. For control and treated cells, MnCV/MnFV ratios are significantly smaller than one at low driving pressures and increase roughly toward one with increasing driving pressures. Lat-A treated cells are characterized by a high MnCV/MnFV (~0.7) at the lowest applied driving pressure as compared to control cells (MnCV/MnFV~0.35), whereas Jpk-treated cells have the lowest MnCV/MnFV (~0.1). Clearly, our microfluidic setup allows us to gain insight into the different degrees of resistance to cell transit in the capillary. Also, the MnCV/MnFV ratios of Blb-treated cells were very similar to control cells for all pressure drops. These results suggest that friction between circulating leukocytes and capillary walls is hardly influenced by myosin activity and is strongly dependent on actin cytoskeleton organization.

Myosin II activity controls the sequestered cell membrane unfolding

To obtain further insight into the sequestered cell morphology, we monitored the maximum axial length, L_m, of the cells in the constriction. No significant evolution of L_m was observed during the cell transit, suggesting that L_m depends only on the cell entry process. As a morphological reference, we used the puck diameter $D_{pu} = 17$ μm corresponding to a cell of initial diameter $D_i = 12$ μm squeezed

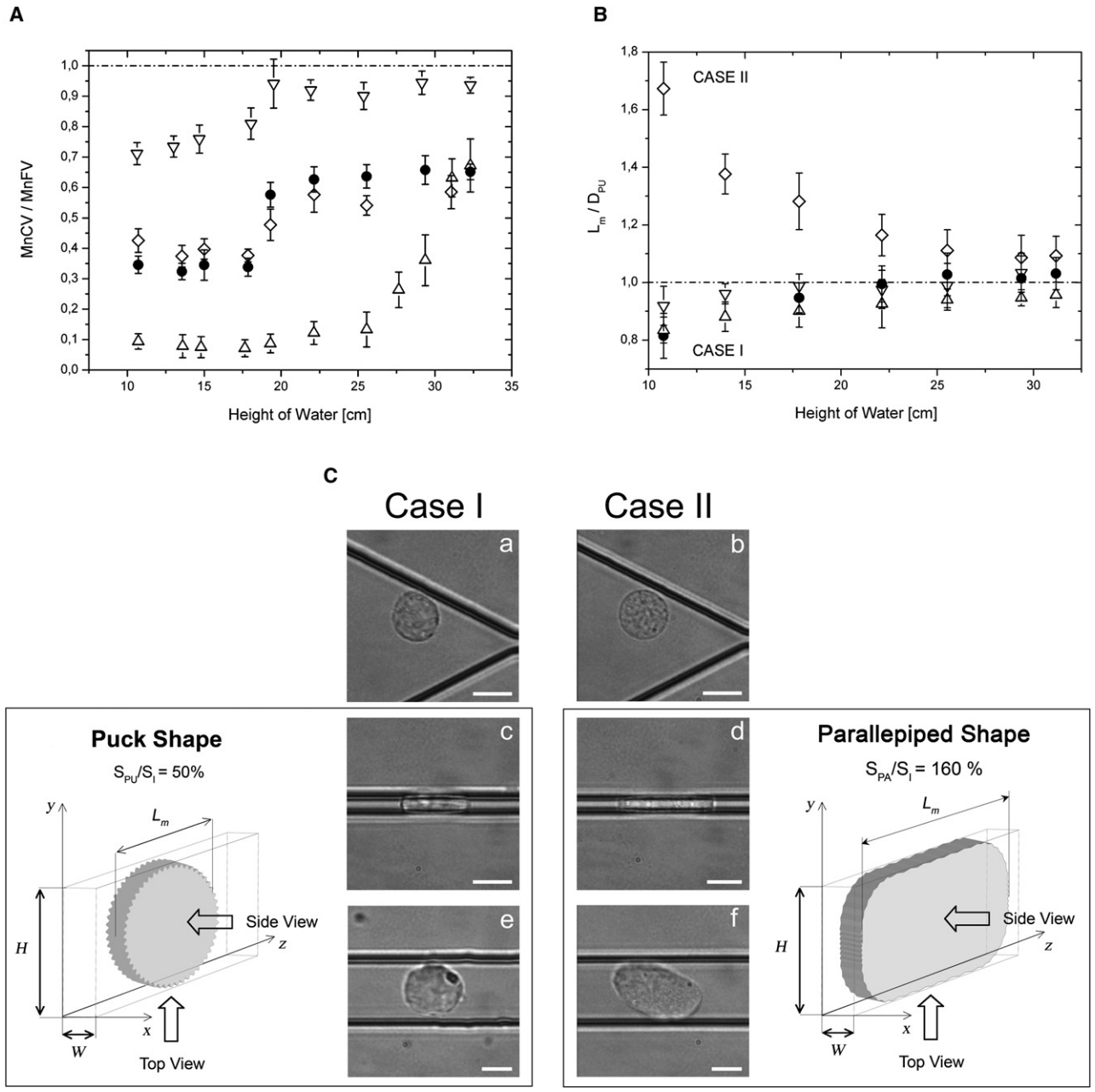

FIGURE 3 Transit stage. (*A*) MnCV/MnFV and (*B*) L_m/D_{pu} as a function of the height of water, ΔH, for normal (•), Blb-treated (◇), Jpk-treated (△), and LatA-treated (▽) THP-1 cells. (*C*) Microscope pictures of THP-1 cells before entry into the constriction (*a* and *b*), in the constriction (*c* and *d*), and shortly after their release from the constriction when the free-rotating cell presented a maximum size (*e* and *f*). Pictures *c* and *d* give respectively insight into the top- and side-views of the cell in the constriction. Case I: Control and Jpk- and Lat-A-treated cells have a puck shape with diameter = 17 μm, height $W = 4$ μm, and excess surface area $\Delta S/S = 50\%$ for all ΔH (*left cartoon*). Case II: Blb-treated cells have a roughly parallelepipedic shape with dimensions of 4, 16, and 29 μm, and excess surface area $\Delta S/S = 160\%$ at $\Delta H = 10.8$ cm H_2O (*right cartoon*). Scale bars on pictures represent 10 μm.

between parallel walls distant of $W = 4$ μm (see Materials and Methods section). Two different trends can be distinguished on Fig. 3 *B*. The first behavior corresponds to control, Jpk-treated, and Lat-A-treated cells, for which L_m/D_{pu} is always close to one. The second behavior corresponds to Blb-treated cells, for which L_m/D_{pu} is always >1 and reaches a maximal value of 1.7 at the lowest applied driving pressure. This finding suggests that only Blb-treated cells exceed the minimal deformation into a puck of diameter D_{pu} and height W. To determine the exact morphology of confined cells, we need to get access to a side view of the cell. This side view can be obtained in the relaxation channel, where released cells rotate freely, allowing access to new angles of sight on the deformed cells (Movie S2). A good approximation of a side view of a confined cell was obtained from the image of the released cell corresponding to

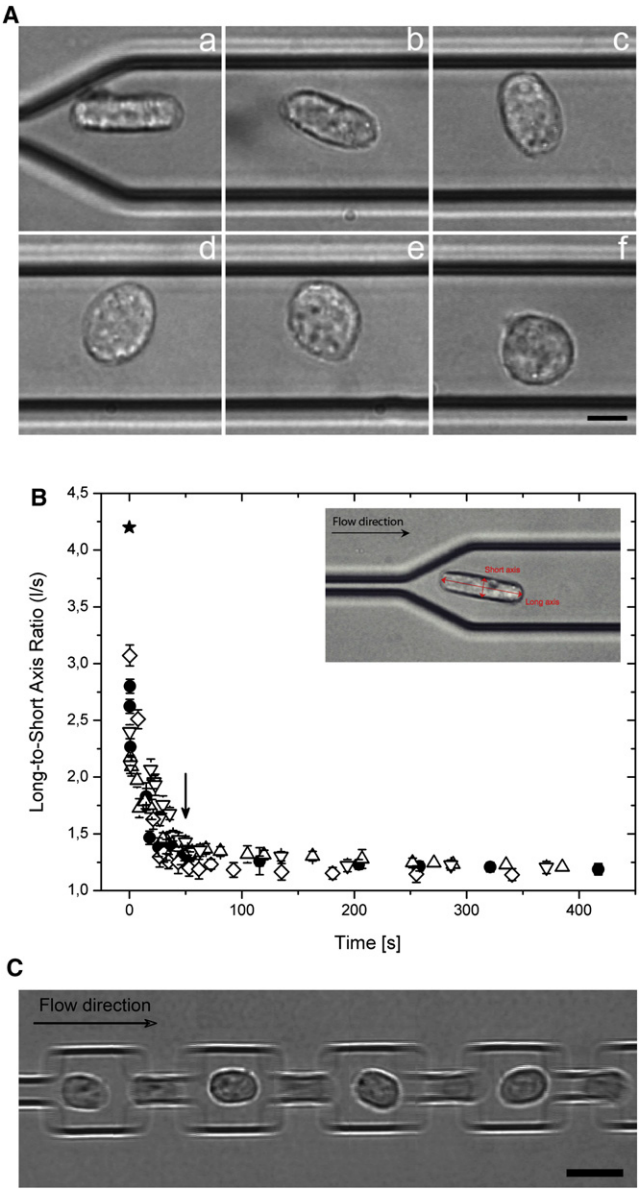

FIGURE 4 Shape relaxation stage. (*A*) Image sequence of a THP-1 cell at different times after release from a 4-μm-wide constriction (*a*) $t = 0.6$ s, (*b*) $t = 7.2$ s, (*c*) $t = 26$ s, (*d*) $t = 41.7$ s, (*e*) $t = 204.3$ s, and (*f*) $t = 413.5$ s. The scale bar represents 8 μm. (*B*) Long/short-axis ratio (l/s) of a THP-1 cell versus the time after release from a 4-μm-wide constriction. Error bars represent SE (THP-1 (●): $n = 4$, LatA (▽): $n = 3$, Jpk (△): $n = 4$, Blb (◇): $n = 3$). The ★ sign at $t = 0$ corresponds to the theoretical l/s ratio of a puck with diameter 16.8 μm and height $W = 4$ μm. The inset shows long (l) and short (s) axes on a picture of a deformed cell. (*C*) Series of images showing the passage of a single THP-1 cell through a succession of 5-μm-wide segments. Scale bar represents 15 μm.

a maximum area. The delay after release of the side-view pictures (~1 s) was short compared to the shape recovery time (~50 s), ensuring that the cell morphology was still close to the morphology in the constriction. Fig. 3 *C* shows sequences of three microscopic pictures for cells 1), in the inlet channel (pictures *a* and *b*); 2), in the constriction channel (pictures *c* and *d*); and 3), in the relaxation channel shortly after release (pictures *e* and *f*). These images correspond respectively to the undeformed spherical cell, the top view, and the side view of the sequestered cell. The morphologies observed for normal and Jpk- and LatA-treated cells (Fig. 3 *C*, *case I*) are all similar and correspond well to a puck of diameter D_{pu} and width W, i.e., to the minimal geometric deformation required for a sphere to enter our microfluidic constriction. The ratio between the cell surface in the puck shape, S_{pu}, and in the initial spherical shape, S_i, can be determined using Eq. 2:

$$S_{pu}/S_i = \frac{D_i}{3W} + \sqrt{\frac{2W}{3D_i}}. \quad (2)$$

S_{pu}/S_i is ~1.5, which corresponds to an excess of cell membrane surface of 50% in the deformed state of case I. On the other hand, the image sequence of case II in Fig. 3 *C* is typical of a Blb-treated cell in the constriction at a low applied driving pressure (13.7 cm H_2O). The cell morphology in the constriction corresponds roughly to a parallelepiped with rounded edges of dimensions 4, 16, and 29 μm. The cross-section dimension 4 × 16 μm of the deformed cell matches the cross-section $W \times H$ of the constriction because the cell expansion is obviously frustrated in directions perpendicular to the constriction main axis. The ratio between the cell surface in its parallelepipedic shape, S_{pa}, and its initial spherical shape, S_i, is expressed by Eq. 3:

$$S_{pa}/S_i = 2\left(\frac{HW + WL_m + HL_m}{\pi D_i^2}\right). \quad (3)$$

S_{pa}/S_i is ~2.6, which corresponds to an excess of cell membrane surface of 160% in the deformed state for the cells of case II in Fig. 3 *B*. These data suggest that, at low applied pressures, inhibition of molecular motors induces a large cell surface increase as compared with the minimal surface increase required to enter the constriction.

Actin organization and actomyosin activity do not influence the shape recovery process

After the cells crossed the 4-μm-wide constriction, they were released into a 20-μm-wide channel, which allowed us to observe the shape relaxation free of external constraints (Fig. 4 *A*). We studied the kinetics of shape recovery quantitatively by monitoring the long/short-axis ratio (l/s; *inset* of Fig. 4 *B*). Since the cell can rotate in the relaxation channel, one must take care to select only pictures corresponding to the same angle of view. The temporal evolution of l/s is presented in Fig. 4 *B* for control and treated cells. The effect of F-actin stabilization (with Jpk), actin disruption (with LatA), or myosin II activity inhibition (with Blb) does not affect the dynamics of leukocyte shape recovery as compared with the unstimulated control groups (THP-1). Furthermore, the

shape is characterized by a fast relaxation (~50 s) of l/s down to 1.3 (which corresponds to the image of Fig. 4 *Ad*) for control and Jpk-, LatA-, and Blb-treated cells (Fig. 4 *B*).

Transit through successive capillary segments

In vivo, leukocytes cross between 50 and 100 segments in a single passage through the highly interconnected pulmonary microvasculature (29). To approach physiological geometries, a long, single capillary was exchanged for a succession of short, narrow segments of width 5 μm and length 20 μm (30). A typical sequence of transit through these segments is presented in Fig. 4 *C* (see Movie S3). The ET is ~25 s in the first constriction and 0.5 s in all subsequent constrictions. This illustrates that a deformed shape (l/s ~ 1.5) facilitates leukocyte transit through the capillary network.

DISCUSSION

Accumulation of leukocytes in pulmonary microvessels (31) is implicated in the pathophysiology of a number of diseases. However, the direct study of leukocyte retention in human microvasculature is a difficult task. Several micromanipulation techniques have enabled the mechanical behavior of nonadherent cells to be studied in vitro. Micropipette aspiration permits investigators to mimic cell deformation in the capillary entry stage, but not to study other stages of cell passage, such as transit dynamics. Polycarbonate filter experiments allow researchers to quantify cell transit times through narrow pores, but not to observe cells in the pores. Our microfluidic experiments allowed us to study and observe at the single-cell level the entry, transit, and shape relaxation stages of leukocyte passage in a constriction. Our 4-μm-wide constrictions aim to mimic human pulmonary capillaries, whose radii vary from 1 to 7.5 μm, with a mean of 3.7 μm (32). Our setup also mimics physiological flow conditions by maintaining constant hydrostatic pressure over time (33).

Previous studies have raised questions regarding the precise role of actin organization and molecular motor activity in the mechanical behavior of leukocytes during their passage in the microvasculature. Actin filaments are a primary structural determinant of cell mechanical properties (14), and leukocytes from patients with sepsis shock and ARDS are abnormally rigid and exhibit an actin-enriched rim in the submembrane region (15,34). On the other hand, myosin II activity plays a role in the mechanical properties of eukaryotic cells (35–37), in the passage of leukocytes through narrow gaps via squeezing contractions during transmigration (18), and in the blebbing motility of leukocytes confined in two or three dimensions (38). Therefore, in this work we investigated the role of actin organization and myosin II activity in the passage of cells through a microfluidic capillary by exposing the cells to specific inhibitors of actin polymerization/depolymerization (LatA and Jpk) and myosin II activity (Blb).

Passive actin cytoskeleton reorganization controls capillary entry

The projection length L_m versus the time in the constriction entry stage follows a sigmoidal curve, which is consistent with investigations of leukocyte deformation with micropipette aspiration (10). This validates the microfluidic approach as an efficient technique to study the mechanical behavior of circulating cells. A key observation is that spherical leukocytes need a finite time to deform and enter the constriction. The presence of the nucleus may a priori contribute to the lack of deformability of leukocytes, especially in the case of our monocytic cell line THP-1, because the constriction width is close to the mean diameter of a monocytic nucleus (39). However, the results observed with LatA-treated cells demonstrate that leukocytes with disrupted microfilaments enter the constriction in very short times (Fig. 2 *B*), even at low applied driving forces. This indicates that the mechanical behavior of leukocytes in our 4-μm-wide constrictions is independent of the viscoelastic nucleus. Moreover, our results show that large deformations are facilitated by disruption of actin filament organization, and that the retardation of cell transit increases with actin polymerization. Leukocytes must reorganize their actin cytoskeleton to enter into microcapillaries. On the other hand, our data obtained from Blb-treated leukocytes, for which ATPase activity was reduced to 5% of the initial value (22), indicate that a drastic reduction of actomyosin activity reduces the ET only slightly. This is consistent with the slight decrease of actin cytoskeleton stiffness reported by Martens and Radmacher (37) on myosin II-inhibited fibroblasts. However, the contribution of myosin II for the cell entry stage is certainly weak in comparison with the large importance of actin microfilament organization. This confirms the conclusion of Yap and Kamm (16) that the ET behaves in a manner consistent with a passive cell.

Actin cytoskeleton controls pressure and friction with capillary walls

Previous studies of cell transit in capillaries reported that the strength of the pressure-drop force F_p pushing the cells through the capillary dominated the friction force F_f resulting from hydrodynamic forces between the cell and the capillary walls (16,29). Our microfluidic experiments were designed to access flow conditions in which the relative strength of F_f against F_p is high enough to observe deviations of cell velocities from mean fluid velocity. Our results can be compared with those obtained by Shao and Hochmuth (40) in a study focusing on flow resistance of leukocytes in glass micropipettes. In the absence of nonspecific adhesion (checked in our experiments on static settled cells), there

are no physical contacts between the moving cells and the channel walls, and thus friction is due only to shear stress in the lubrication film between the cell and the walls. In vivo, the gap between a trafficking cell and the endothelium is composed of two layers. Close to the wall, the endothelial glycocalyx layer has a thickness of ~500 nm (41). Between the glycocalyx and the trafficking cell, the lubrication layer of thickness 15–100 nm (40) contains only medium fluid. The flow of liquid in the glycocalyx layer was shown to be low as compared with the flow in the lubrication layer (42). Therefore, the fluid velocity gradient and hydrodynamic shear stress between the cells and walls in vivo occurs mainly in the lubrication layer. In our experiments with artificial walls, there is a lubrication layer and no endothelial glycocalyx layer. Nevertheless, since friction arises mainly from the hydrodynamic shearing in the lubrication layer, the force F_f is expected to be comparable in vivo and in our microfabricated channels. Only the effects of glycocalyx layer compliance under stress (41) are not taken into account in our experiments. For a given cell and capillary geometry, the dependance of the ratio between the friction force F_f and the pressure force F_p against the driving pressure ΔP is given by

$$\frac{F_f}{F_p} \propto \frac{v}{\Delta P \delta}, \tag{4}$$

where v is the cell velocity, ΔP is the applied pressure, and δ is the lubrication film thickness. The velocity v being proportional to ΔP (when friction forces are negligible), and the lubrication layer thickness δ varying as a power law of velocity with an exponent 2/3 (43), $\frac{F_f}{F_p}$ epends on velocity as

$$\frac{F_f}{F_p} \propto \frac{1}{v^{2/3}}. \tag{5}$$

Equation 5 shows that the relative importance of F_f against F_p decreases with velocity. Friction forces are therefore negligible at high driving pressures, and cell velocity is controlled by pressure forces only. This explains why, in Fig. 3 *A*, all MnCV/MnFV ratios tend roughly toward one for high ΔP. Conversely, at low driving pressures and low cell velocities, the relative effects of friction are enhanced, which explains why we observe various behaviors. For a given channel geometry and applied driving pressure, the main parameter controlling the strength of F_f is the lubrication film thickness, δ (40). A lower cell velocity can be attributed to a thinner lubrication layer, and therefore to a higher pressure exerted by the cell against the walls. Using this point of view, several pieces of information can be obtained in the transit stage from the cell velocity differences. First, Newtonian liquid drops with the same volume, same surface tension, and different viscosities would experience the same lubrication conditions and thus would have the same velocities. Therefore, only the elasticity of the membrane and/or the cytoplasm can explain transit velocity differences. Many micropipette investigations have already demonstrated viscoelastic effects on the leukocyte entry stage in a capillary (44). We present here the first evidence (to our knowledge) that viscoelastic effects also play a significant role in leukocyte transit through a narrow capillary. Second, the fact that Jpk- and LatA-treated cells exert respectively higher and lower pressures on the walls as compared to normal cells demonstrates that the cell elastic component exerting a pressure on the walls arises significantly from the actin network organization. Third, the velocity results provide direct proof that the rheological state of normal and Jpk- and LatA-treated cells differs in the constriction for the different treatments. Strong deformation rates or shear stresses are known to significantly decrease cells' elastic moduli (16,45). This effect may also occur in our experiments, but the velocity results prove that the forced entry of normal and Jpk-treated cells in narrow constrictions does not completely disrupt their actin scaffold. On the other hand, we found that myosin II activity does not significantly influence velocity and friction. In the end, friction is strongly influenced by actin network organization and hardly by myosin II activity, exactly like stiffness. This further supports the idea that stiffness and friction are highly correlated: the membrane of stiffer cells (Jpk treated > normal > LatA treated cells) is pushed harder on the walls, and thus the lubrication film is thinner and friction higher.

Membrane unfolding: myosin II activity contributes to microvilli zipping

Excess leukocyte plasma membrane area is stored in folds and villi (46), and it was recently suggested that wrinkles are stabilized by membrane-cytoskeleton-membrane bonds (47). During the deformation of a spherical cell, membrane area is recruited from this reservoir by wrinkles smoothing out, e.g., during phagocytosis (48) or squeezing in a constriction. In our experiments, the deformation process occurs during the entry stage only. Of interest, normal leukocytes in the constriction exhibit a minimal deformation from a sphere to a puck. This implies the existence of a mechanism that resists excess membrane unfolding. Herant et al. (47) observed a similar resistance to membrane area expansion against osmotic pressure. They introduced the concept of a ''molecular velcro'' mechanism that holds wrinkles together and whose molecular nature remains largely unknown (49). We have seen that Jpk- and LatA-treated cells behave like controls. This demonstrates that alteration of actin filaments does not play a significant role in the resistance to cell membrane unfolding, at least in the range of stresses applied here.

On the other hand, Blb-treated cells exhibit a large excess unfolding under similar applied stress. The surface increase for Blb-treated cells in the 4-μm-wide capillary reached 160%, whereas minimal deformation to enter the constriction corresponds to 50%. This demonstrates that the mechanism

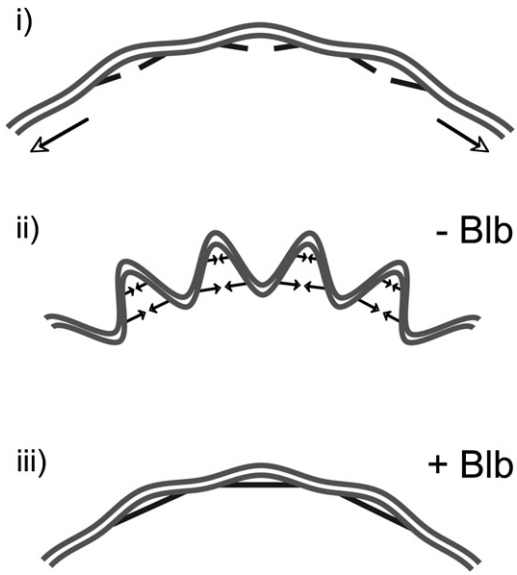

FIGURE 5 Scheme of the actomyosin activity contribution to membrane folding. (*i*) Cell membrane after a large expansion. Microvilli are unfolded and membrane-cytoskeleton-membrane links are cleaved. (*ii*) Normal cells: links rebuild and myosin II exerts tension (arrows) to rewrinkle the membrane. (*iii*) Blb-treated cells: without myosin II tensile activity links may re-form, but the membrane is not wrinkled after 30 s.

for resisting membrane unfolding involves myosin II activity. Moreover, the membrane area increase of 160% is comparable to the maximum excess area determined by micropipettes experiments (50). This suggests that Blb-treated cells have unfolded the totality of their reservoir membrane wrinkles, and that wrinkle velcro gripping is largely weakened with Blb treatment. This raises an important question: Does the role of myosin II in velcro gripping consist of reinforcing the static strength or in accelerating the dynamic re-formation of new links and wrinkles? The exact function of myosins is not completely understood, but myosin II is always associated with contractile activity, such as cytokinesis (pinning apart of a dividing cell) or migration (forward translocation of the body of a cell). The contractile function suggests that myosin II may participate in membrane wrinkling by pulling on actin filaments anchored at different points of the membrane. Following this hypothesis, it is interesting to note that not all Blb-treated cells exhibit a maximum unfolding. Blb-treated cells at the highest applied driving pressure exhibit minimal membrane unfolding (a surface area increase of 50%), exactly like control cells. This proves that wrinkle grips still exist in Blb-treated leukocytes before application of a mechanical stress/deformation. Since Blb blocks myosin in an actin-detached state, there are probably other cross-linking molecules, such as talin or ezrin, that maintain wrinkle gripping (49). It is also important to note that velcro unzipping takes place at the lowest mechanical stress intensity. This further supports the idea that velcro ungripping is not attributable to a decrease in the static gripping strength, but rather to a dynamic effect. In Fig. 3 *B*, the onset of L_m/D_{pu} for Blb-treated cells starts at $\Delta H < 20$–25 cm/H_2O, which corresponds to ETs of >30 s. This indicates that the characteristic time required for velcro detachment is ~30 s. More importantly, this indicates also that the characteristic time required for wrinkle re-formation is <30 s in Blb-treated cells; otherwise, the unfolded state could not be seen. This conclusion strongly suggests that myosin II activity is directly involved in the dynamic mechanism of wrinkle re-formation, and that this mechanism is not fast enough in Blb-treated cells to compensate for the increase in membrane surface. This confirms the hypothesis that myosin II is involved in the dynamics of wrinkle re-formation, most probably by exerting forces between different anchoring points on the membrane (Fig. 5).

Membrane unfolding has not been investigated in pulmonary diseases implicating leukocyte sequestration. Most investigators have focused on cell mechanical and adhesive properties (51). It has been established that the first leukocyte/endothelium contacts are mediated by selectins and their counterreceptors (52), and that known adhesion molecules (L-selectin, P-selectin, and CD11/CD18) have no role in the initial sequestration (4,53). Our experiments confirm that cell stiffness can contribute to initial sequestration, which supports the notion that adhesion is not required. On the other hand, we determined a characteristic time for membrane velcro unzipping of ~30 s, so that arrested cells in vivo undergo hydrodynamic stresses on a time span long enough to permit membrane unfolding. Moreover, cell activation due to deformation (54) and/or local inflammation can further promote membrane unfolding (55), like the Blb treatment in our experiments. A full understanding of the biochemical and mechanical events that occur during sequestration has not emerged yet; however, our results suggest that membrane unfolding may play an important role in leukocyte-endothelial cell interactions by mediating or aggravating the inflammatory processes.

Deformation threshold for leukocyte activation

Cell velocity was found to be constant for all cells during cell transit in constrictions. Also, the formation of pseudopods after passage in constrictions was observed in <10% of assays with normal and LatA- and Jpk-treated cells. The forced passage in our constrictions is therefore a poor trigger of cell activation. This is consistent with the proposition by Yap and Kamm (54) that activation (pseudopod formation) occurs only above a deformation threshold. If one defines S_f/S_i as the ratio of the final cell surface area S_f over the initial cell surface area S_i, they found that neutrophil activation occurs for $S_f/S_i = 1.86$ and not for $S_f/S_i = 1.26$. In our experiments, $S_f/S_i = 1.5$ for normal and LatA- and Jpk-treated cells, and 10% of the cells activated. It makes sense to say that S_f/S_i is below the threshold. Conversely, for Blb-treated cells, we found that $S_f/S_i = 2.6$, which is clearly above the threshold. In this case, ~80% of the cells activated.

Actin and actomyosin activity do not drive the cell shape recovery

When a leukocyte is expelled from a narrow capillary into a larger channel, it almost recovers its initial spherical shape in a characteristic time of 50 s, which is in agreement with previous observations (56). A remarkable result is that the shape recovery process is unaffected by perturbations of actin organization or actomyosin activity. Normal and treated cells undergo a similar shape recovery. Moreover, this shape recovery is independent of the duration of sequestration in the capillary. These results raise a question as to the origin of the driving force leading to the shape relaxation, since it cannot be ascribed to actin polymerization or to actomyosin activity. On the other hand, it is interesting to recall that velocity measurements have shown that the viscoelastic properties of normal and Jpk- and LatA-treated cells were very different after their forced passage in the constriction. One can then conclude that the mechanism driving cell shape relaxation is robust enough to dominate the effect of different viscoelastic properties of cells with different actin cytoskeleton organizations. A mechanism that drives the global cell shape and applies forces on a scale of several microns requires the (re)building of a large macromolecular scaffold. The three major filamentous constituents of the cytoskeleton are potentially involved in the constitution of this scaffold. Our results obtained with Jpk- and LatA-treated cells provide the first piece of evidence, to our knowledge, that actin is not dominantly involved in cell shape relaxation. Others have already presented results suggesting that microtubules play a negligible role in the mechanical properties of circulating leukocytes (57,58). This leaves intermediate filaments as the most probable actor in cell shape recovery after deformation. It is interesting to note that this conclusion is consistent with recent experiments demonstrating that vimentin intermediate filaments are the main contributors to the stiffness of circulating lymphocytes (13). Our results strongly suggest that the specific role of intermediate filaments in the different stages of leukocyte trafficking in capillaries should be further investigated (59).

A deformed leukocyte state helps normal trafficking through the capillary bed

The kinetics of cell relaxation helps to shed light on the behavior of leukocytes in pulmonary transit, where the pathway from an arteriole to a venule consists of 50–100 connected constriction segments (29) and the transit time has been measured in vivo at a median value of 26 s, with very large deviations (60). The characteristic shape recovery time of 50 s observed in our experiments is of particular interest. This time does not allow complete shape recovery between two successive segments; however, a deformed shape may facilitate the leukocytes' transit through subsequent restrictions imposed by the capillary bed.

CONCLUSIONS

We used a microfluidic technique to investigate the passage of leukocytes in a narrow capillary, which is the starting event of postsepsis or trauma disorders in the lung microvasculature. This in vitro and single-cell approach provides an improved understanding of the role of actin and myosin II in capillary leukocyte trafficking under physiologically relevant mechanical and hydrodynamical conditions. We have established that molecular motor activity and the redistribution of actin filaments have specific and different roles in the extent and rate of cell deformation and cell membrane unfolding in the different stages (i.e., the entry stage, transit stage, and shape recovery stage) of leukocyte trafficking in a constriction. Leukocyte ET into a capillary, and hydrodynamic friction with the capillary walls are strongly enhanced by the degree of actin polymerization. This confirms the important role of the actin network organization in the sequestration of leukocytes in capillaries. To our knowledge, our results also provide the first assessment of the contribution of myosin II activity to cellular transit in narrow capillaries. Myosin II activity only marginally influences the global cell mechanical properties, but appears to be a key element in the mechanism of membrane unfolding under stress. Finally, the cell shape recovery time of 50 s was shown to significantly help the transit through the capillary segment network. Of importance, we also showed that the characteristic time of cell shape recovery is not driven by actin polymerization or actomyosin activity, which suggests that the role of intermediate filaments should be systematically investigated at each stage of traffic through a capillary.

SUPPORTING MATERIAL

Three movies and a figure are available at http://www.biophysj.org/biophysj/supplemental/S0006-3495(09)00598-0.

The authors thank the Rhodia Company (Lab of the Future, Pessac, France) for technical support with microfabrication and financial support of S.G.'s postdoctoral fellowship.

REFERENCES

1. Frutos-Vivar, F., N. Nin, and A. Esteban. 2004. Epidemiology of acute lung injury and acute respiratory distress syndrome. *Curr. Opin. Crit. Care.* 10:1–6.
2. Schmid-Schönbein, G. W. 1987. Capillary plugging by granulocytes and the no-reflow phenomenon in the microcirculation. *Fed. Proc.* 46:2397–2401.
3. Worthen, G. S., B. Schwab, E. L. Elson, and G. P. Downey. 1989. Mechanism of simulated neutrophils: cell stiffening induces retention in capillaries. *Science.* 245:183–186.
4. Yoshida, K., R. Kondo, Q. Wang, and C. M. Doerschuk. 2006. Neutrophil cytoskeletal rearrangements during capillary sequestration in bacterial pneumonia in rats. *Am. J. Respir. Crit. Care Med.* 174:689–698.
5. Petersen, N. O., W. B. McConnaughey, and E. L. Elson. 1982. Dependence of locally measured cellular deformability on position on the cell, temperature and Cytochalasin B. *Proc. Natl. Acad. Sci. USA.* 79:5327–5331.

6. Franck, R. S. 1990. Time-dependent alterations in the deformability of human neutrophils in response to chemotactic activation. *Blood*. 76:2606–2612.
7. Thoumine, O., and J. Ott. 1997. Time scale dependent viscoelastic and contractile regimes in fibroblasts probed by microplate manipulation. *J. Cell Sci.* 110:2109–2116.
8. Rotsch, C., and M. Radmacher. 2000. Drug-induced changes of cytoskeletal structure and mechanics in fibroblasts—an atomic force microscopy study. *Biophys. J.* 78:520–535.
9. Sheetz, M. P. 1998. Laser Tweezers in Cell Biology. Academic Press, London, UK.
10. Chien, S., K. L. Sung, G. W. Schmid-Schonbein, R. Skalak, E. A. Schmalzer, et al. 1987. Rheology of leukocytes. *Ann. N.Y. Acad. Sci.* 516:333–347.
11. Fabry, B. B., G. N. Maksym, J. P. Butler, M. Glogauer, D. Navajas, et al. 2003. Time scale and other invariants of integrative mechanical behavior in living cells. *Phys. Rev. E. Nonlin. Soft Matter Phys.* 68:041914.
12. Balland, M., N. Desprat, D. Icard, S. Féréol, A. Asnacios, et al. 2006. Power laws in microrheology experiments on living cells: comparative analysis and modeling. *Phys. Rev. E. Stat. Nonlin. Soft Matter Phys.* 74:021911.
13. Brown, M. J., J. A. Hallam, E. Colucci-Guyon, and S. Shaw. 2001. Rigidity of circulating lymphocytes is primarily conferred by vimentin intermediate filaments. *J. Immunol.* 166:6640–6646.
14. Sheikh, S., W. B. Gratzer, J. C. Pinder, and B. Nash. 1997. Actin polymerization regulates integrin-mediated adhesion as well as rigidity of neutrophils. *Biochem. Biophys. Res. Commun.* 238:910–915.
15. Nishino, N., H. Tanaka, H. Ogura, Y. Inoue, T. Koh, et al. 2005. Serial changes in leukocytes deformability and whole blood rheology in patients with sepsis or trauma. *J. Trauma*. 59:1425–1431.
16. Yap, B., and R. D. Kamm. 2005. Mechanical deformation of neutrophils into narrow channels induces pseudopods projection and changes in biomechanical properties. *J. Appl. Physiol.* 98:1930–1939.
17. Pai, A., P. Sundd, and D. F. J. Tees. 2008. In situ microrheologial determination of neutrophil stiffening following adhesion in a model capillary. *Ann. Biomed. Eng.* 36:596–603.
18. Lämmermann, T., B. L. Bader, S. J. Monkley, T. Worbs, R. Wedlich-Söldner, et al. 2008. Rapid leukocyte migration by integrin-independent flowing and squeezing. *Nature*. 453:51–55.
19. Rosenbluth, M. J., W. A. Lam, and D. A. Fletcher. 2008. Analyzing cell mechanics in hematologic diseases with microfluidic biophysical flow cytometry. *Lab Chip*. 8:1062–1070.
20. Wong, P. K., W. Tan, and C.-M. Ho. 2005. Cell relaxation after electrodeformation: effect of latrunculin A on cytoskeletal actin. *J. Biomech.* 38:529–535.
21. Bubb, M. R., A. M. Senderowicz, E. A. Sausville, K. L. Duncan, and E. D. Korn. 1994. Jasplakinolide, a cytotoxic natural product, induces actin polymerization and competitively inhibits the binding of phalloidin to F-actin. *J. Biol. Chem.* 269:14869–14871.
22. Straight, A. F., A. Cheung, J. Limouze, I. Chen, N. J. Westwood, et al. 2003. Dissecting temporal and spatial control of cytokinesis with a myosin II inhibitor. *Science*. 299:1743–1747.
23. Tsuchiya, S., M. Yamabe, Y. Yamaguchi, Y. Kobayashi, T. Konno, et al. 1980. Establishment and characterization of a human acute monocytic leukemia cell line (THP-1). *Int. J. Cancer*. 26:171–176.
24. Vitte, J., A.-M. Benoliel, P. Eymeric, P. Bongrand, and A. Pierres. 2004. β1 integrin-mediated adhesion may be initiated by multiple incomplete bonds, thus accounting for the functional importance of receptor clustering. *Biophys. J.* 86:4059–4074.
25. Samaniego, R., L. Sánchez-Martín, A. Estecha, and P. Sánchez-Mateos. 2007. Rho/ROCK and myosin II control the polarized distribution of endocytic clathrin structures at the uropod of moving T lymphocytes. *J. Cell Sci.* 120:3534–3543.
26. Joanna, C., J. C. Porter, M. Bracke, A. Smith, D. Davies, et al. 2002. Signaling through integrin LFA-1 leads to filamentous actin polymerization and remodeling, resulting in enhanced T cell adhesion. *J. Immunol.* 168:6330–6335.
27. Xia, Y., and G. M. Whitesides. 1998. Soft lithography. *Angew. Chem. Int. Ed.* 37:550–575.
28. Tabeling, P. 2005. Introduction to Microfluidics. Oxford University Press, London, UK.
29. Bathe, M., A. Shirai, C. M. Doerschuk, and R. D. Kamm. 2002. Neutrophil transit times through pulmonary capillaries: the effects of capillary geometry and fMLP-stimulation. *Biophys. J.* 83:1917–1933.
30. Weibel, E. R. 1963. Morphometry of the Human Lung. Academic Press, New York.
31. Downey, G. P., and G. S. Worthen. 1988. Neutrophil retention within model capillairies: role of the cell deformability, geometry and hydrodynamic forces. *J. Appl. Physiol.* 65:1861–1871.
32. Doerschuk, C. M., N. Beyers, H. O. Coxson, B. Wiggs, and J. C. Hogg. 1993. Comparison of neutrophil and capillary diameters and their relation to neutrophil sequestration in the lung. *J. Appl. Physiol.* 74:3040–3045.
33. Huang, Y., C. M. Doerschuk, and R. D. Kamm. 2001. Computational modeling of RBC and neutrophils transit through the pulmonary capillary. *J. Appl. Physiol.* 90:545–564.
34. Skoutelis, A. T., V. Kaleridis, G. M. Athanassiou, K. I. Kokkinis, Y. F. Missirlis, et al. 2000. Neutrophil deformability in patients with sepsis, septic shock, and adult respiratory distress syndrome. *Crit. Care Med.* 28:2355–2359.
35. Jay, P. Y., P. A. Pham, S. A. Wong, and E. L. Elson. 1995. A mechanical function of myosin II in cell motility. *J. Cell Sci.* 108:387–393.
36. Wakatsuki, T., R. B. Wysolmerski, and E. L. Elson. 2003. Mechanics of cell spreading: role of myosin II. *J. Cell Sci.* 116:1617–1625.
37. Martens, J. C., and M. Radmacher. 2008. Softening of the actin cytoskeleton by inhibition of myosin II. *Pflugers Arch.* 456:95–100.
38. Charras, G., and E. Paluch. 2008. Blebs lead the way: how to migrate without lamellipodia. *Nat. Rev. Mol. Cell Biol.* 9:730–736.
39. Schmid-Schönbein, G. W., Y. Y. Shih, and S. Chien. 1980. Morphometry of human leukocytes. *Blood*. 56:866–875.
40. Shao, J.-Y., and R. M. Hochmuth. 1997. The resistance to flow of individual human neutrophil in glass capillary tubes with diameters between 4.65 μm and 7.74 μm. *Microcirculation*. 4:61–74.
41. Vink, H., and B. R. Duling. 1996. Indentification of distinct luminal domains for macromolecules, erythrocytes, and leukocytes within mammalian capillaries. *Circ. Res.* 79:581–589.
42. Damiano, E. R. 1998. The effect of the endothelial-cell glycocalyx on the motion of red blood cells through capillaries. *Microvasc. Res.* 55:77–91.
43. Bico, J., and D. Quéré. 2002. Self-propelling slugs. *J. Fluid Mech.* 467:101–127.
44. Sung, K. L. P., C. Dong, G. W. Schmid-Schönbein, S. Chien, and R. Skalak. 1988. Leukocyte relaxation properties. *Biophys. J.* 54:331–336.
45. Trepat, X., L. Deng, S. S. An, D. Navajas, D. J. Tschumperlin, et al. 2007. Universal physical responses to stretch in the living cells. *Nature*. 447:592–596.
46. Bessis, M. 1973. Living Blood Cells and Their Ultrastructure. Springer, Berlin.
47. Herant, M., W. A. Marganski, and M. Dembo. 2003. The mechanics of neutrophils: synthetic modeling of three experiments. *Biophys. J.* 84:3389–3413.
48. Simon, S. I., and G. W. Schmid-Schönbein. 1988. Biophysical aspects of microsphere engulfment by human neutrophils. *Biophys. J.* 53: 163–173.
49. Dewitt, S., and M. Halett. 2007. Leukocyte membrane ''expansion'': a central mechanism for leukocyte extravasation. *J. Leukoc. Biol.* 81:1160–1164.
50. Raucher, D., and M. P. Sheetz. 1999. Characteristics of a membrane reservoir buffering membrane tension. *Biophys. J.* 77:1992–2002.

51. Doerschuk, C. M. 2001. Mechanisms of leukocyte sequestration in inflamed lungs. *Microcirculation.* 8:71–88.

52. Kansas, G. S. 1996. Selectins and their ligands: current concepts and controversies. *Blood.* 88:3259–3287.

53. Wang, Q., E. T. Chiang, M. Lim, J. Lai, R. Rogers, et al. 2001. Changes in the biomechanical properties of neutrophils ans endothelial cells during adhesion. *Blood.* 97:660–668.

54. Yap, B., and R. D. Kamm. 2005. Cytoskeletal remodeling and cellular activation during deformation of neutrophils into narrow channels. *J. Appl. Physiol.* 99:2323–2330.

55. Herant, M., V. Heinrich, and M. Dembo. 2005. Mechanics of neutrophil phagocytosis: behavior of the cortical tension. *J. Cell Sci.* 118:1789–1797.

56. Tran-Son-Tay, R., D. Needham, A. Yeung, and R. M. Hochmuth. 1991. Time-dependent recovery of passive neutrophils after large deformation. *Biophys. J.* 60:856–866.

57. Hofman, P., L. d'Andrea, E. Guzman, E. Selva, G. Le Negrate, et al. 1999. Neutrophil F-actin and myosin but not microtubules functionally regulate transepithelial migration induced by interleukin 8 across a cultured intestinal epithelial monolayer. *Eur. Cytokine Netw.* 10: 227–236.

58. Saito, H., J. Lai, R. Rogers, and C. M. Doerschuk. 2002. Mechanical properties of rat bone marrow and circulating neutrophils and their responses to inflammatory mediators. *Blood.* 99:2207–2213.

59. Chou, Y.-H., F. W. Flitney, L. Chang, M. Mendez, B. Grin, et al. 2007. The motility and dynamic properties of intermediate filaments and their constituent proteins. *Exp. Cell Res.* 313:2236–2243.

60. Lien, D. C., W. W. Wagner, Jr., R. L. Capen, C. Haslett, W. L. Hanson, et al. 1987. Physiologic neutrophil sequestration in the canine pulmonary circulation. *J. Appl. Physiol.* 62:1236–1243.